Sub-millisecond electron density profile measurement at the JET tokamak with the fast lithium beam emission spectroscopy system

Sub-millisecond electron density profile measurement at the JET tokamak with the fast Lithium Beam Emission Spectroscopy system

D.I. Réfy,[1] M. Brix,[2] R. Gomes,[3] B. Tál,[1] S. Zoletnik,[1] D. Dunai,[1] G. Kocsis,[1] S. Kálvin,[1] T. Szabolics,[1] and JET Contributors[a)]

[1)] *Wigner Research Centre for Physics, 1121 Budapest, XII. Konkoly Thege Miklós út 29-33., Budapest, Hungary*

[2)] *CCFE, Culham Science Centre, Abingdon, Oxon, OX14 3DB, UK,*

[3)] *Instituto de Plasmas e Fusão Nuclear, Instituto Superior Técnico, Universidade de Lisboa, 1049-001 Lisboa, Portugal*

Diagnostic alkali atom (e. g. Lithium) beams are routinely used to diagnose magnetically confined plasmas, namely to measure plasma electron density profile in the edge and the scrape off layer (SOL) region. The principle of such beam emission spectroscopy (BES) diagnostic is as follows. The beam atoms collide with plasma particles which excite and ionize them. Spontaneous decay of beam atoms results in a characteristic photon emission that can be detected through an optical system. The electron density distribution can be calculated from the measured light emission distribution along the beam (light profile). A light splitting optics system was installed into the Li-BES observation system at the JET tokamak, which allows simultaneous measurement of the beam light emission with a spectrometer and a fast avalanche photo diode camera (APDCAM). The spectrometer measurement allows density profile reconstruction with 10 ms time resolution, absolute position calculation from the Doppler shift, spectral background subtraction as well as relative intensity calibration of the channels for each discharge. The APD system is capable of measuring light intensities on the microsecond time scale. However $\sim 100\mu$s integration is needed to have acceptable signal to noise ratio (SNR) due to moderate light levels. Fast modulation (up to 30 kHz) of the beam is implemented which allows background subtraction on the 100μs time scale. An automated routine has been developed which does the background subtraction, the relative calibration, the comprehensive error calculation, runs a Bayesian density reconstruction code and loads results to the JET database. The paper demonstrates the capability of the APD system by analyzing fast phenomena like pellet injection and ELMs.

I. INTRODUCTION

The Joint European Torus (JET) is the largest tokamak experiment which utilizes numerous plasma diagnostics in order to monitor as many plasma parameters as possible. The JET device is equipped with a Lithium beam emission spectroscopy (Li-BES) system[1], which is a routinely used diagnostic of magnetically confined plasmas.

The working principle of such a diagnostic can be summarized as follows. An accelerated atomic beam is injected into to plasma, where the beam atoms are excited and ionized by plasma particles. The ionization process results in a gradual loss of the atoms in the beam. The ionization rate is such that the beam can penetrate only the edge of the plasma, thus Li-BES systems are used for electron density profile and fluctuation measurement of the outer plasma regions only, namely the plasma edge and scrape off layer (SOL).

Spontaneous de-excitation of the beam atoms results in a characteristic photon emission at 670.8 nm that can be detected through an optical system. The distribution of the light emission along the beam (light profile) can be measured with a detector system, from which the electron density distribution (density profile) can be calculated[2,3]. An important feature of such a diagnostic is that the beam attenuation sets the absolute magnitude of the plasma electron density, thus only relative calibration of the light profile is needed.

Prior to the system upgrade in 2012, the JET Li-BES system consisted of an ion gun, and an observation system, in which a spectrometer measured the narrowband spectral distribution of the beam light emission at 24 locations along the beam. It was observed that even an upgraded spectrometer can process only about 10% of the light collected by the optics, therefore a light splitting optics and a 32 channel avalanche photodiode camera (APDCAM[4]) was installed to process the remaining 90% of the light[5]. To further increase system capabilities a fast beam modulation system and an ion source upgrade was also done[6]. In this paper we describe the density profile measurement capabilities of the avalanche photodiode system.

The paper is organized as follows. A brief overview of the hardware setup is shown in section II, focusing on the elements those are critical for this paper. Section III describes the steps of the lightprofile calculation, namely the problem of background correction (Sec. III A), the relative calibration (Sec. III B) and the error calculation (Sec. III C). Section IV introduces the density reconstruction method and its validation at JET. Two examples are shown in section V to demonstrate the capabilities of the system, namely a temporally resolved ELM

[a)] See the author list of Overview of the JET results in support to ITER by X. Litaudon et al. to be published in Nuclear Fusion Special issue: overview and summary reports from the 26th Fusion Energy Conference (Kyoto, Japan, 17-22 October 2016)

(edge localized mode) event, and a pellet injection.

II. DIAGNOSTIC SETUP

The Li-BES system consists of a Lithium beam injector and an observation system.

The former contains a thermionic ion source, an ion optics, two pairs of electrode plates for beam alignment and deflection, a Sodium vapor neutralizer and a flight tube, and it is located on the top of the JET tokamak, shooting vertically down. The thermionic ion source emits ions when it is heated to ∼1300°C and an extraction voltage is present. It is mounted in the Pierce electrode from which a two stage ion optics extracts, accelerates and focuses the Lithium ions to 60keV energy. The beam can be aligned and chopped (deflected so as the beam does not enter the plasma) by applying a voltage on the deflection plates. The chopping is needed to be able to distinguish between the Lithium emission and the background. The neutralizer is a Sodium filled oven which produces sodium vapor when it is heated to ∼250°C. The Lithium ions are neutralized by charge exchange process passing through the neutralizer. The Lithium beam injector has an Iron shield up to the neutralizer to keep the external magnetic field out of the region of the ion beam. The Lithium atoms are injected into the plasma through the flight tube.

The JET Lithium beam injector is a version of the original ASDEX Lithium beam design[7], and has been recently upgraded. The upgrade concerned the ion source[6], and is capable of producing 1-2mA equivalent beam current in plasma. This upgrade also included the development of the beam deflection system[8] which is now capable of chopping the beam up to 30 kHz.

The observation system can be divided into two parts; one is the periscope on the machine, inside the torus hall that images the beam emission on a fibre array through an adjustable mirror and an optical system. The beam is observed from a quasi-tangential view looking downwards onto the beam at 0-45 degree angle. The image diameter of the fibres on the beam is 6-10 mm, depending on location. The mirror is located in the far SOL, thus it is time to time subject to reflection loss due to deposited layers. This part can be replaced during a shutdown using the remote handling arm. The other part, which is in an optical enclosure in the diagnostic hall, processes the light trasmitted by the 65 optical fibres, those diameter is 1 mm. This part has been upgraded as well in 2012[5], and was equipped with a light splitting optical system that divides the light, coming from the torus hall through fibre optics, between a spectrometer and an avalanche photo diode camera (APDCAM, Fusion Instruments Kft). Light splitting is done with a small mirror in a Fourier plane of the fibres so as the light directed to the spectrometer fills the Numerical Aperture of it. Light which would fall outside of the NA of the spectrometer is directed to the APD camera.

The spectrometer is capable of measuring the light emission from 26 fibres with 10ms time resolution in a 10 nm spectral band. Spectral background correction, relative calibration of the channels after each plasma discharge by shooting into neutral gas and several automated density reconstruction codes are implemented. The spectrometer provides spatial calibration as well, since the position of the measurement along the beam can be calculated from the Doppler shift of the line emission, and the observation geometry. This proved to be necessary as the periscope mirror position setting is somewhat unsure due to mechanical hysteresis and thermal expansion.

The APDCAM has 32 APD detectors out of which 26 measure the light from the same input fibres as the spectrometer, i.e. these channels are measured simultaneously by the two systems. The APDCAM system is optimized for the relatively low light intensities, set to 250 kHz analogue bandwidth, and measures with 500 kHz sampling. The time resolution of the system is limited by the signal to noise ratio (SNR) which is in the range of 1-10 along the beam, when the ion gun is at its peak performance. This means that the relative error (statistical fluctuation of the light level) of the measurement can be reduced to an acceptable 5% level by 0.1-1 ms integration, since the error is inversely proportional to the square root of the number of independent measurement points.

III. LIGHT PROFILE CALCULATION

The fast density deconvolution requires the calculation of a relatively calibrated beam light profile. In order to achieve this, the handling of the background light, the relative calibration of the channels and the calculation of the errors is necessary. This section will show the steps of this analysis.

A. Background correction

The APD branch of the observation system is equipped with an interference filter with FWHM=2.4nm, which is needed due to the wide wavelength range of the Doppler-shift of the beam emission. This wide interference filter cannot fully suppress the broadband radiation of the plasma which acts as a background to our measurement. The signal-to-background ratio (SBR) of the system is in the range of 3-12, and is not homogeneous along the observation range, thus has to be taken into account. This can be carried out by the modulation of the beam (chopping). The time scale on which the background light is taken into account, namely the half period time of the chopping determines the maximum time resolution of the system. The background correction becomes unreliable in case of fast transient events those modulate the

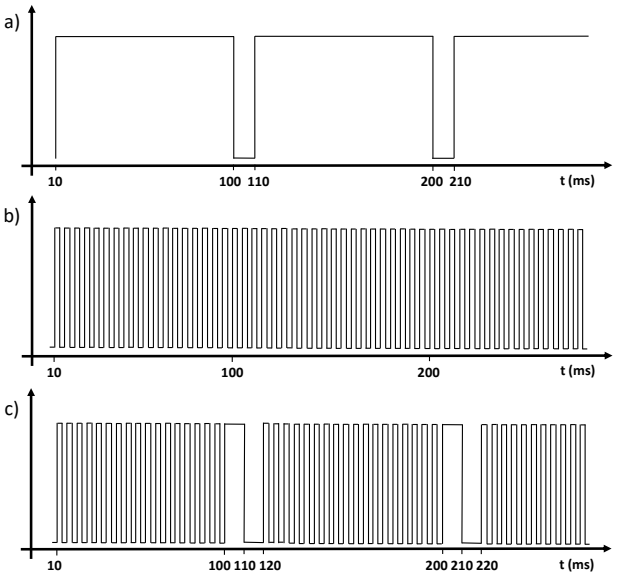

FIG. 1: Three beam modulation modes are illustrated: slow modulation (a), fast modulation (b) and mixed modulation (c) mode. The fast modulation period time is not to scale, it is in the 100μs range.

background on a timescale comparable to the chopping frequency.

Three chopping modes are available: slow modulation, when the beam is chopped out for each e.g. 10th camera frame synchronized with the 10ms long camera frame time, fast modulation, when the beam is continuously chopped with up to 30 kHz frequency and mixed modulation, when the beam is on for every e.g. 10th camera frame, off for the next frame to have sufficient background measurement for the spectrometer, and fast modulation in between. The three chopping modes are illustrated in Figure 1, note that the intervals with fast modulation are not to scale.

The background is calculated from each beam-off time interval, interpolated for the beam-on intervals and subtracted from the signal level.

B. Relative calibration

The background corrected light intensity is proportional to the beam emission in the observed volume multiplied by the solid angle of the observation, the transmission of the observation system, the detection efficiency, the fibres and the interference filter. The density profile calculation does not require the absolute value of the light intensity, as it was mentioned above, just the relative light intensity distribution along the beam (light profile), thus the relative calibration factors have to be determined[3]. Two methods are implemented.

The first calculates the calibration factors from a measurement in which the beam is injected into neutral gas where the beam emission can be considered homogeneous. In this case, the relative calibration factors are simply inversely proportional to the measured intensity. The spectrometer branch is calibrated after each plasma discharge with this method. The neutral gas pressure from the outgassing of the walls is sufficiently high to get reasonable signal on the spectrometer with 0.5s integration time. As the SNR of the APD branch in the gas measurement is low (0.1-1), this method can be used if the beam performs well, a sufficiently long ($\sim$3s) beam into gas shot takes place after the discharge and the periscope mirror is clean.

Due to the limitations of the gas calibration another method was implemented, based on the following considerations. The two branches of the detection system are measuring the same input light intensities, and thus can be cross calibrated. This is carried out by matching the background corrected (spectral correction for the spectrometer, correction as described in Section III A for the APDCAM) light level in a plasma shot in the two systems for each channel, in a carefully chosen time interval, where no events are present which modulate the background too fast (i.e. faster than the 10ms time scale of the spectrometer frame time). Typically a few 100ms long L-mode part of a discharge is sufficient for this purpose.

C. Error calculation

In order to perform a density calculation from the light profile, errors should be quantified through a comprehensive error calculation, taking all sources into account, those are the following.

- Random error
  - Electonic noise of the APD camera amplifiers
  - Photon noise from plasma background
  - Photon noise from Lithium emission
- Systematic error
  - Gas calibration error
  - Cross calibration error

The electronic noise and the photon noise are the random error sources in our measurement. The first step of the evaluation is a signal to noise curve calculation from the raw signal. The noise spectrum is measured at different light levels by illuminating the APD detectors with a LED light source. This confirmed that the spectrum of both the electronic and the photon statistical noise is flat from about 1kHz up to the bandwidth. The power in the 100-150kHz range of the signal spectra is considered purely electronic and photon noise (e.g. no plasma background or beam light fluctuations are expected in this frequency range), thus the total electronic and photon noise is calculated by the linear extrapolation of this

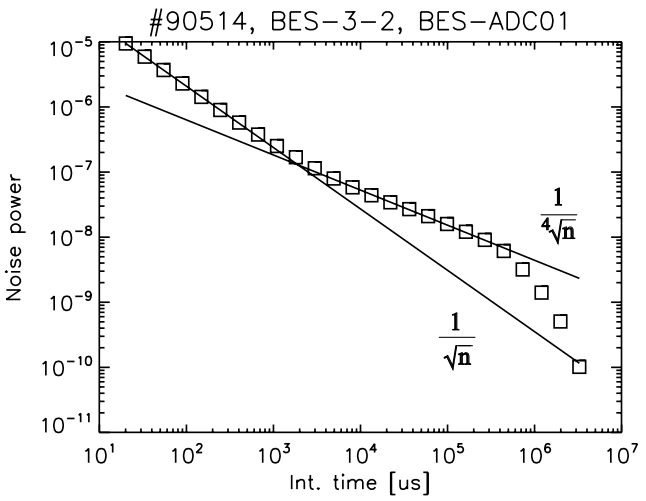

FIG. 2: The power in the signal as a function of integration time. Above 2ms integration time, the low frequency noise dominates the power, and the power falls only with the fourth root of the sample number.

power for the total 250kHz analogue bandwidth. The photon noise has Poisson statistics, thus the variance and the mean of the raw signal are proportional when there is light on the detector. The variance and the mean of the raw signal is calculated in each e.g. 1 millisecond during the plasma discharge, and the result signal to noise curve is fitted with a linear function. This method is applied for each channel, and the result fits give the noise level for any signal level and channel in the examined plasma shot. This way we can define the random error level for each sample of the APDCAM.

During the background subtraction the error propagation rules are taken into consideration. For a given beam-on interval, the background is the average of the mean light levels in the neighboring beam-off intervals. The error of the mean background adds to the mean signal error squared. At this point one has the non-calibrated Lithium light level and the random error for each beam-on time.

The two types of relative calibration, described in Section III B brings systematic error into the calculation.

Error calculation for the APD system gas calibration is critical as the ∼1mV signal level during gas shot is small compared to the ∼10mV electronic noise. The photon statistical noise is negligible at this light level.

The standard error of the mean in case of white noise decreases with the square root of the sample number, but a detailed analysis showed, that the error decreases with the fourth root of the number of averaged samples above ∼2ms integration time. The effect is illustrated in Figure 2 where the fluctuation power of an APD signal is indicated as a function of the integration time for a beam-on interval. The increased noise level is due to the offset drift and pick-up noise that dominates the white noise at low frequency.

Taking this into consideration the error of the gas calibration is calculated as follows. The APD data is recorded before, during and after the ∼2s long beam injection into neutral gas, and the beam on and the beam off phases are divided into N equidistant, ∼100ms long parts each, and averaged within these intervals. N is chosen to have a fair statistics, 16 in our case. The error of a detector signal is then described by equation 1, where $\sigma(t_{on})$ and $\sigma(t_{off})$ are the standard deviation of the N element vector of beam intensities during beam on and beam off phases respectively. The standard error calculated this way will be referred to as modified standard error (MSE).

$$\mathrm{MSE} = \frac{\sqrt{\sigma^2(t_{on}) + \sigma^2(t_{on})}}{\sqrt[4]{N}} \tag{1}$$

The error of the cross calibration is calculated as follows. The calibrated Lithium light level of a spectrometer channel is read from the JET database, while the APD data of the corresponding input fibre is averaged over each 10ms long spectrometer frame time in the same time range. This way one has the time evolution of the Lithium light in both systems with identical sampling, and the time trace of the calibration factor can be achieved by dividing one vector by the other. The modified standard error of this timetrace gives the error of the cross calibration factor. The discussion of the spectrometer system calibration error is out of the scope of this paper. It was found to be negligible compared to other error sources, and thus not taken into account.

After these considerations, one have both the random and the systematic error for each APD sample, those can be added up squared following the error propagation rules. In case of temporal integration of the signal, the two errors are handled separately, and the systematic error is added only after the standard error of the mean have been calculated. The integration takes only the independent data points into consideration, which is calculated from the analogue bandwidth and the integration time range.

The results of the calibration methods and the error calculation can be seen in Figure 3. In this paper, ρ_{pol} refers to rho poloidal, the normalised magnetic flux coordinate. The normalized lightprofiles calculated with gas and cross calibration are shown with red and green line, the spectrometer profile is indicated with blue line, while the dashed lines indicate the one sigma errors of the profiles, respectively. It has to be emphasized, that this gas calibration precision can be reached only with sufficiently high nautral gas pressure, that can be achieved by a dedicated gas calibration pulse. Yet no dedicated gas pulse is available at JET after the plasma shots, the gas calibration is carried out usually in the gas from the recombined plasma and the outgassing of the walls. The possibility of active gas injection after plasma termination is being investigated to increase the signal level during the gas calibration.

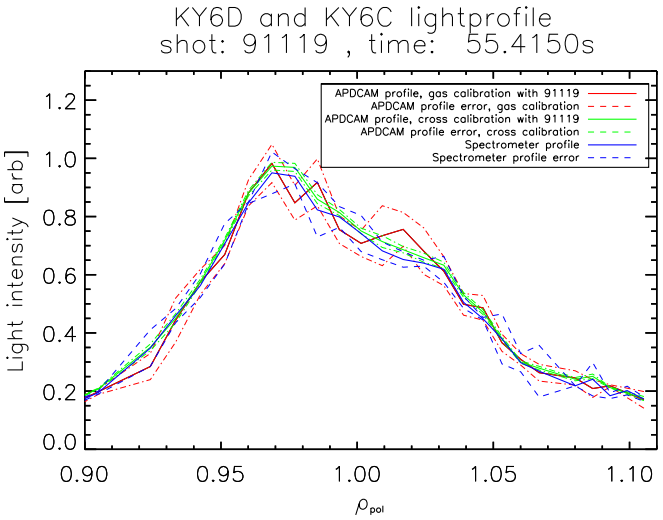

FIG. 3: JET light emission profile calculated from the gas calibrated (red line) and cross calibrated (green line) APDCAM data, and from the spectrometer data (blue line). Dashed lines show the errors correspondingly.

IV. DENSITY PROFILE RECONSTRUCTION

A Bayesian density profile calculation method was implemented and validated against the numerical implementation of the method described in Ref[3] on ASDEX Upgrade data. The code is written in IDL and utilizes the atomic physics core of the RENATE BES simulator[9,10].

The atomic physics of the beam can be discussed within the collisional-radiative model. The light profile and the density profile are connected through the rate equations which is a coupled differential equation system. The integration is straightforward if one wants to calculate the light profile from a given density profile. One solution for the inverse problem is based on the Bayesian Probability Theory, that is search the most probable density profile for a given light profile. Similarly to Ref[3] we describe the probability of a density profile as a product of the likelihood of the forward calculated light profile and some prior probability. For the likelihood of the forward calculated light profile a Gaussian likelihood is assumed around the measured light profile with the error estimates as standard deviation. The prior reduces the unphysical density profiles. Weak monotonicity conditions are applied, that is a mostly monotonically increasing density profile towards the plasma center is assumed. The second prior penalizes the curvature of the density profile, that is the reconstruction gives a smooth density profile. This prior pdf mainly acts as a weak constraint to the space of density profiles consistent with physical considerations. The advantage of this reconstruction method is that can be applied to noisy data as in the case of the APDCAM measurement.

The error of the density profile is calculated by applying a local gaussian density perturbantion and increasing its amplitude while the $\tilde{\chi}^2$ of the forward calculated light profile changes by 1. The local perturbed density at this setting is considered as the 1σ error at the given location. It has to be emphasized, that the error calculated this way is not a local error, since a local density perturbation influences the whole light profile after the perturbation through the atomic physics.

As a first step validation of the density calculation we compared the results with density profiles calculated from spectrometer data. In Figure 1, blue line shows the density profile measured by the spectrometer, reconstructed by a non statistical, standard JET Li-BES reconstruction method[2], while red line shows the density profile measured by the APDCAM, reconstructed by the Bayesian method in the same time interval and time resolution (10ms) for an L-mode case in Figure 4 (a) and for a H-mode case in Figure 4 (b).

As a second step validation we compared the density profiles with other electron density measurements at JET. Figure 5 shows the electron density profile measured with four diagnostics: the Lithium beam data calculated from the APDCAM is indicated with light blue triangles, while from the spectrometer with redtriangles, the core Thomson scattering is shown with black plus signs while the high resolution Thomson scattering with dark blue diamonds, each mapped on the equatorial plane. The radial coordinate of the Lithium beam was shifted by 3cm inwards to match the pedestal position, this is due to a known discepancy of the EFIT and being investigated. The profiles show a fairly good agreement up to the pedestal top ($\rho_{pol} \simeq 0.95$), while Li-BES looses sensitivity thereafter due to ionization, and the reconstruction stops.

V. DENSITY PROFILE MEASUREMENT EXAMPLES

The temporal and spatial resolution of the JET Li-BES diagnostic is to be demonstrated in this chapter. Two temporally resolved fast events, an ELM crash and a pellet injection case are presented in this section.

A. ELM cycle

Edge Localized Modes (ELMs) are fast, periodic plasma events in H-mode, that are of interest due to their role played in impurity transport and the high particle and heat load carried by them which is hazardous in terms of machine operation and safety.[11] Figure 6(a) shows the time evolution of the density profile determined with the method presented above between 2 ELMs as a contour plot. The x axis is time [s], the y axis is the height above mid-plane coordinate [m] along the beam which propagates downwards. The previous ELM event and the pedestal build up can be seen in the region marked with green, inter-ELM phase is marked with blue, while the pedestal crashes and the density profile flattens due

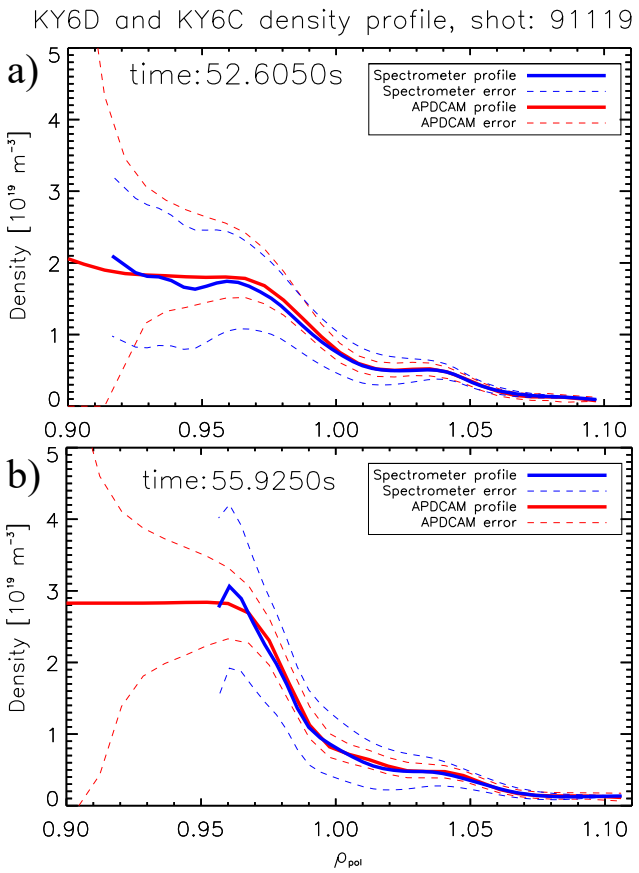

FIG. 4: JET density profile calculated from the spectrometer data (blue line) and from APDCAM data (red line) for (a) L-mode, and (b) H-mode case. Dashed lines show the errors correspondingly.

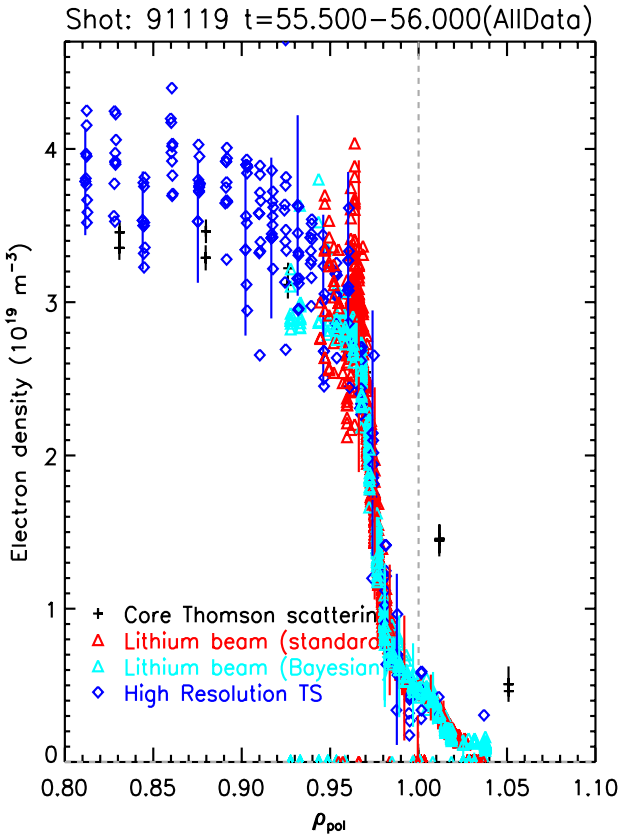

FIG. 5: JET density profile calculated from the APD data with our Bayesian code (light blue), from spectrometer data with a deterministic code (red), core Thomson scattering diagnostic (black) and high resolution Thomson scattering diagnostic (dark blue) .

to the ELM in the region marked with red. The increased SOL density corresponds to outward particle flux due to the ELM. The last closed flux surface (LCFS) is marked with a white dashed line. The inner divertor Beryllium signal is shown as a reference in Figure 6(b), where the increased load due to the ELM event is immediate on the density measurement time scale. The density profiles during the ELM crash (solid line) and the corresponding errors (dotted line) are shown in Figure 6(c). The color of the profiles correspond to the vertical dashed lines in Figure 6(a,b) showing the time of selected profile. First the pedestal top density is decreased by 20%, while the density in the SOL is increased which correspond to the ELM induced outward particle flux. It worthwhile to point out that the error of the density profile at a given radial position is increased by a factor two during the ELM due to the increased background light.

B. Pellet injection

Pellet injection is recognized as an important tool for plasma fuelling and ELM control. To understand the underlying processes of the pellet ablation and particle deposition it is of interest to detect the pellet caused density increase on the time scale of a few tens of microseconds. Pellets can trigger ELMs in H-mode plasmas therefore to disentangle the effect of fuelling and density change caused by the triggered ELMs, the dynamics of the pellet caused density profile change was investigated in L-mode discharges. The pellet injection was carried out with the low field side pellet injector. As a typical example Figure 7(a) shows the density change relative to the average density over the investigated interval at different radial locations. The pellet ablation monitor (D-alpha light) is also plotted in Figure 7(b) as a reference. The pellet induced density increase propagating into the plasma (marked by dotted line) is clearly seen on Figure 7(a). The marked peak is propagating with about 100m/s speed (5cm/500μs) which is in the order of the typical pellet speed. Figure 7(c) shows the density profiles (solid line) and the corresponding errors (dotted line) at the time slices indicated in figure 7(a,b) revealing also the above mentioned density increase propagating into the plasma. The effect of the electron temperature change was investigated, and was found to be negligable

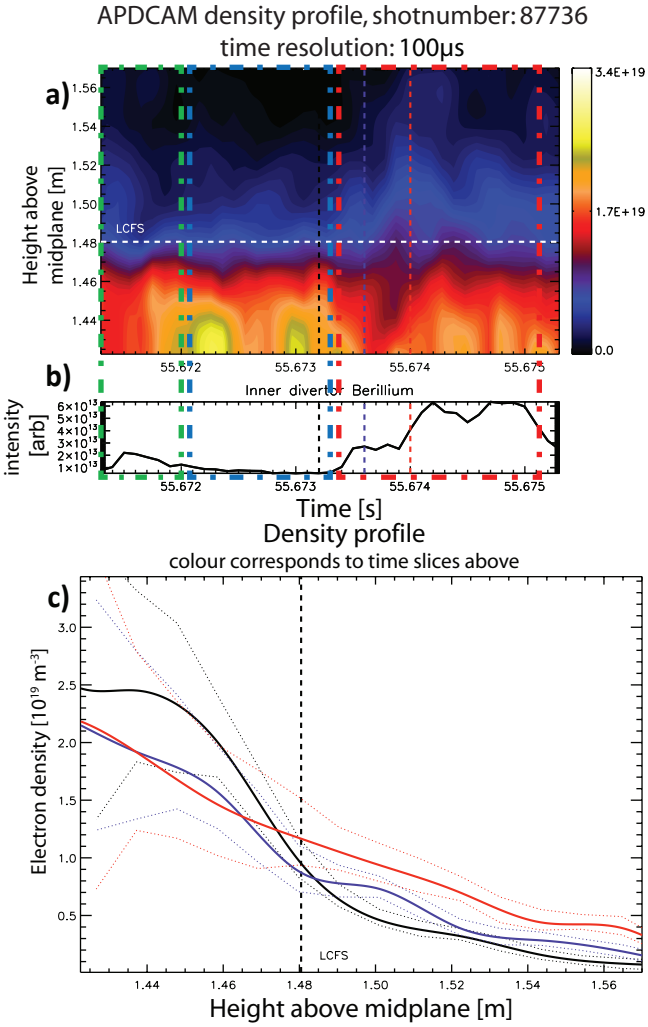

FIG. 6: Temporally resolved ELM crash: (a) contour plot of the density profile time evolution, (b) inner divertor Berillium signal, (c) density profile at the selected time slices (solid line) and the corresponding errors (dotted line). The colored dashed-dotted windows in the contour plot marks 3 periods of the ELM cycle. The previous ELM and the density pedestal build up is marked with green, the inter ELM phase is marked with blue and the temporally resolved ELM event is marked with red.

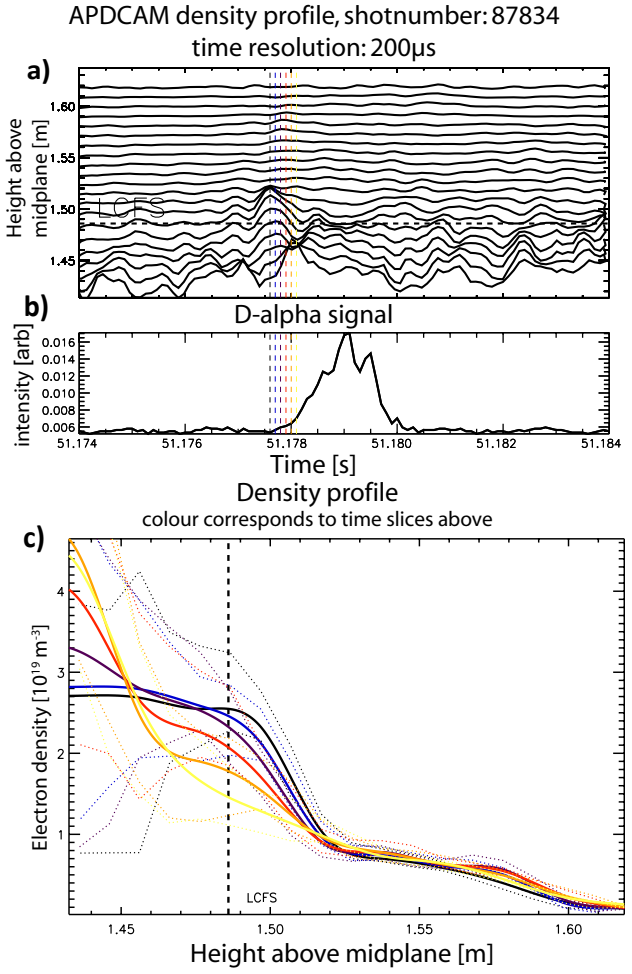

FIG. 7: Temporally resolved pellet penetration: (a) level plot of the density profile time evolution, (b) divertor D-alpha signal below, (c) density profile at the selected time slices (solid line) and the corresponding errors (dotted line). Level plot interpretation: each line represents the time trace of the density relative to the average density over the whole interval at a fixed radial position.

even in this case, when the edge temperature decreases by a factor 4 (from 200eV to 50eV) during the fast event.

VI. SUMMARY AND CONCLUSIONS

The Li-BES system at the JET tokamak is a routinely used diagnostic for electron density profile measurement. The device has been upgraded in the recent years, and a fast beam emission light detection system was implemented. The fast background correction through chopping of the beam, and the simultaneous measurement of the beam emission light with the APDCAM and the spectrometer system enables us to produce ∼1cm spatial and ∼100μs temporal resolution SOL and plasma edge density profiles up to the pedestal top. The temporal resolution is a factor 100 improvement compared to prior the system upgrade.

Comparing to a recent upgrade of the ASDEX Upgrade Li-beam system[12,13] one can observe that the light intensity in the fast branch is similar, therefore the time resolution of the two diagnostics are also similar. The distinct feature of the JET Li-beam system is the faster chopper which enables precise background measurement on a 100 microsecond timescale.

On the other hand the SNR of the JET Li-beam diagnostic does not allow measurement on a timescale below 100μs, thus zonal flow and edge turbulence measurements

like on TEXTOR[14] are still not possible. Determining SOL and edge turbulence spectra and correlation functions like on ASDEX Upgrade[13] and Wendelstein 7-AS[15] are possible and will be reported in a separate paper.

This feature of the system enables us to resolve the evolution of fast transient events, such as ELM-s, pellet injection, L-H transition and M-mode[16], which are in the focus of interest at magnetically confined devices.

ACKNOWLEDGMENTS

This work has been carried out within the framework of the EUROfusion Consortium and has received funding from the Euratom research and training programme 2014-2018 under grant agreement No 633053. The views and opinions expressed herein do not necessarily reflect those of the European Commission.

[1] M. Brix, A. Korotkov, M. Lehnen, P. Morgan, K. McCormick, J. Schweinzer, D. Summers, and J. Vince, *Proc. 28th Conf. on Control. Fusion Plasma Phys.(Madeira) Europhys. Conf. Abstracts A*, **25**, 389 (2001).

[2] J. Schweinzer, E. Wolfrum, F. Aumayr, M. Pockl, H. Winter, R. P. Schorn, E. Hintz, and A. Unterreiter, Plasma Physics and Controlled Fusion **34**, 1173 (1992).

[3] R. Fischer, E. Wolfrum, J. Schweinzer, and the ASDEX Upgrade Team, Plasma Physics and Controlled Fusion **50**, 085009 (2008).

[4] A. R. Field, D. Dunai, R. Gaffka, Y.-c. Ghim, I. Kiss, B. Meszaros, T. Krizsanoczi, S. Shibaev, and S. Zoletnik, Review of Scientific Instruments **83**, 013508 (2012).

[5] M. Brix, D. Dodt, D. Dunai, I. Lupelli, S. Marsen, T. Melson, B. Meszaros, P. Morgan, G. Petravich, D. Refy, *et al.*, Review of Scientific Instruments **83**, 10D533 (2012).

[6] G. Bodnar, S. Bat, S. Zoletnik, M. Brix, and R. Gomes, JET internal report **EFDAJETCP(14)05/11** (2014).

[7] K. McCormick, S. Fiedler, G. Kocsis, J. Schweinzer, and S. Zoletnik, Fusion Engineering and Design **34-35**, 125 (1997).

[8] S. Zoletnik, G. Petravich, A. Bencze, M. Berta, S. Fiedler, K. McCormick, and J. Schweinzer, Review of Scientific Instruments **76**, 073504 (2005).

[9] D. Guszejnov, G. I. Pokol, I. Pusztai, D. Refy, S. Zoletnik, M. Lampert, and Y. U. Nam, Review of Scientific Instruments **83**, 113501 (2012).

[10] I. Pusztai, G. Pokol, D. Dunai, D. Refy, G. Por, G. Anda, S. Zoletnik, and J. Schweinzer, Review of Scientific Instruments **80**, 083502 (2009).

[11] H. Zohm, Plasma Physics and Controlled Fusion **38**, 105 (1996).

[12] M. Willensdorfer, E. Wolfrum, R. Fischer, J. Schweinzer, M. Sertoli, B. Sieglin, G. Veres, F. Aumayr, and the ASDEX Upgrade Team, Review of Scientific Instruments **83**, 023501 (2012), `http://dx.doi.org/10.1063/1.3682003`.

[13] M. Willensdorfer, G. Birkenmeier, R. Fischer, F. M. Laggner, E. Wolfrum, G. Veres, F. Aumayr, D. Carralero, L. Guimarais, B. Kurzan, and the ASDEX Upgrade Team, Plasma Physics and Controlled Fusion **56**, 025008 (2014).

[14] S. Zoletnik, L. Bardoczi, A. Kraemer-Flecken, Y. Xu, I. Shesterikov, S. Soldatov, G. Anda, D. Dunai, G. Petravich, and the TEXTOR Team, Plasma Physics and Controlled Fusion **54**, 065007 (2012).

[15] S. Zoletnik, M. Anton, M. Endler, S. Fiedler, M. Hirsch, K. McCormick, J. Schweinzer, and the W7-AS Team, Physics of Plasmas **6**, 4239 (1999).

[16] E. R. Solano, N. Vianello, E. Delabie, J. Hillesheim, P. Buratti, D. Refy, I. Balboa, A. Boboc, R. Coelho, B. Sieglin, S. Silburn, P. Drewelow, S. Devaux, D. Dodt, A. Figueiredo, L. Frassinetti, S. Marsen, L. Meneses, C. Maggi, J. Morris, S. Gerasimov, M. Baruzzo, M. Stamp, D. Grist, I. Nunes, F. Rimini, S. Schmuck, I. Lupelli, C. Silva, and J. contributors, Nuclear Fusion **57**, 022021 (2017).